Studies of adsorption processes in the UiO-66 microporous metal-organic framework

Project duration: 03.01.2022–02.01.2023
Project manager: Dr Andrzej Sławek
Academic Centre of Materials and Nanotechnology

AGH University of Krakow

RESEARCH UNIVERSITY EXCELLENCE INITIATIVE

INTRODUCTION:

The aim of the project is to study the physisorption processes in the microporous material UiO-66 (University of Oslo, material number 66) in a hybrid experimental and computational approach. The UiO-66 crystal lattice consists of zirconium clusters [$Zr_6O_4(OH)_4$] linked with bidentate organic ligands of 1,4-dibenzocarboxylic (BDC or terephthalic) acid. The combination of these building units creates a network of interconnected tetrahedral (Ø ≈ 8 Å) and octahedral (Ø ≈ 11 Å) cages. Depending on the conditions of the synthesis, the UiO-66 material may be characterized by a different amount of structural defects. These defects are due to the lack of some organic linkers, which are replaced by hydroxyl groups -OH, while the material maintains its crystal structure. The research hypothesis assumes that the amount of defects in the UiO-66 structure affects the porosity of this material, e.g. the pore volume and BET surface area, as well as the selectivity for adsorption of molecules of different sizes and shapes. Moreover, the presence of additional polar -OH groups should change the nature of this material – from hydrophobic to moderately hydrophilic. This effect should show differences in the properties of UiO-66 for the adsorption of molecules with different dipole moments. According to literature reports, UiO-66 is characterized by reverse selectivity towards hydrocarbons, i.e. it tends to adsorb more branched molecules than those with a linear carbon chain. An interesting aspect of the research is how the selectivity of hydrocarbon adsorption depends on the presence of defects in the UiO-66 crystal lattice and how the number of defects affects the adsorption of polar molecules.

METHODOLOGY:

Various experimental and computational techniques were used in this project:

- The synthesis of a series of UiO-66 samples was carried out. Three UiO-66 preparations were obtained by heating the reagents (BDC:Zr with 2:1 molar ratio) at solvothermal conditions (in a sealed autoclave) at elevated temperatures. The amount of structural defects was controlled by this temperature of 220°C, 160°C or 100 °C.
- Basic physicochemical characterization of the obtained powder materials was performed using a set of experimental techniques: X-ray diffraction (XRD), scanning electron microscopy (SEM) and Fourier-transformed infrared spectroscopy (FT-IR).
- Adsorption isotherms were measured for different polar and non-polar molecules: N_2, Ar, CO_2, CH_4, methanol and ethanol in the studied UiO-66 materials.
- Quasi-equilibrium temperature-programmed desorption and adsorption (QE-TPDA) was used to investigate adsorption of linear and branched hexane isomers in the studied UiO-66 materials.
- *In situ* Fourier-transformed infrared spectroscopy (FT-IR) combined with density functional theory (DFT+D) calculations were used to estimate the preferential adsorption sites for CO_2 and methanol molecules in UiO-66 structures.
- Grand Canonical Monte Carlo (GCMC) calculations were used to model the measured adsorption isotherms/isobars in order to help understand the experimental data.

RESULTS AND DISCUSSION:

We synthesized a series of three materials with the UiO-66 crystal lattice (Figure 1), which was confirmed by the analysis of the XRD patterns (Figure 2). UiO-66_220 C stands for the most ideal material, while UiO-66_100 C for the most defected one. The conducted SEM imaging (Figure 3) shows that the most defected material is characterized by the smallest crystallite size (0.1–0.3 µm) compared to the other samples (0.5–0.9 µm). Apparently, the higher the synthesis temperature, the greater the tendency to aggregate and forming larger crystals.

The presence of structural defects was confirmed by low-pressure adsorption of Ar followed by the analysis of the micropore size distribution using NLDFT technique (Figure 4). It showed that all the studied UiO-66 preparations have micropores of 7 Å and 9.4 Å, which are related to the two types of cavities, but only the defected material possess a significant amount of larger pores of 15.5-18 Å, which correspond to the voids formed by adjacent cavities. The amount of defects was confirmed using the FT-IR spectroscopy (Figure 5) by analyzing the intensity of the band between 2750 and 3750 cm^{-1}, which is derived from the vibrations of hydrogen-bonded physisorbed methanol. The additional -OH groups result from larger amounts of solvent attracted to numerous defects in the preparations.

Adsorption isotherms of N_2 and Ar were also used to calculate the pore volume and the specific surface of the materials, using the t-plot and Brunauer-Emmett-Teller (BET) methods, respectively. As presented in Table 1, voids created by the missing linkers significantly increase the micropore volume and specific surface area of the materials. For comparison, we determined pore volumes for n-hexane (nC6) adsorption that is based on liquid adsorbate. Interestingly, for all materials, the values are ca. 10% higher for N_2 than for nC6, which clearly results from better packing of smaller molecules in the micropores.

Shape selectivity of the studied UiO-66 was investigated based on the adsorption of hexane isomers (Figure 6). Uptake was almost twice as high for the defective material as for the ideal one, while adsorption was shifted towards lower temperatures. Grand Canonical Monte Carlo (GCMC) molecular modeling was used to obtain insight into adsorption at the molecular level. Theoretical force fields were refined to better reflect the experimental data. We found two adsorption states for adsorption of branched hexane isomers in ideal and slightly defected UiO-66 profiles. GCMC simulations revealed that adsorption in ideal UiO-66 takes place only in tetrahedral and octahedral cavities, each of which can contain at most one such molecule. This effect was not observed for the defected UiO-66 preparation.

We also measured and calculated adsorption isotherms of methanol and ethanol (Figure 8 9), to evaluate whether adsorption of polar molecules is similar to that of non-polar ones. Similarly as for alkanes, total uptake increases with the number of defects of UiO-66. However, the adsorption mechanism was found to be completely different. Most of the molecules are adsorbed close to the hydroxyl groups present on the metal clusters and on the created defects, which also induces stronger adsorption manifested by the shift of adsorption isotherms to lower pressures.

CONCLUSIONS:

A wide range of experimental and simulation techniques was exploited to investigate the structure and porosity of the UiO-66 metal–organic framework, with particular emphasis on the presence of defects in the crystal lattice. A series of three UiO-66 preparations was synthesized solvothermally at different temperatures. FT-IR and XRD experimental techniques revealed a different concentration of the missing 1,4-BDC linkers in the obtained preparations.

Adsorption measurements of N_2 and Ar showed type I adsorption isotherms, revealing that micropore volume and specific surface area significantly increase with the number of defects. It was proven that the presence of defects negatively affect the reverse shape-selectivity of hexane isomers in UiO-66. Adsorption of non-polar C6 alkanes in ideal UiO-66 takes place only in tetrahedral and octahedral cavities, each of which can contain at most one such molecule. This results in a low contribution of the guest-guest interactions to the adsorption process. The preferred tetrahedral cages provide suitable voids for bulky molecules, which is responsible for the unusual "reverse" selectivity of UiO-66. The introduction of defects to the crystal lattice causes interconnection of the tetrahedral cavities, which are preferred by linear molecules adhering better to the pore walls. This greatly reduces the selectivity of the material for the branched molecules (Figure 7). It can be concluded that, for the separation of di-branched C6 alkanes, the UiO-66 material should be free from defects in crystal lattice. This process can be effective only in tetrahedral cavities for loadings up to 2/3 of the saturation loading.

We also analyzed the effect of the adsorption of polar, nonpolar and quadruple molecules on UiO-66 structures with changing hydrophobic to hydrophilic character. It was found that, in the case of the nitrogen molecule, the available sites within the cavities are filled only at the highest pressure, governing by the strongest guest-host interactions in smaller tetrahedral cages. For methane and argon, adsorption takes place on all available sites, with no preference for being closer to the metal clusters or -OH groups. In the case of carbon dioxide, the presence of a small number of defects does not significantly affect the shape of the adsorption isotherm, and molecules adsorb mainly on the organic linkers, avoiding adsorption sites close to metal clusters containing -OH groups. For polar molecules such as methanol and ethanol, the mechanism is analogous to that of water. The additional -OH groups introduced at the defect sites attract the molecules, resulting in adsorption at the lowest pressure.

In conclusion, switching the properties of the material from hydrophobic to hydrophilic has no major effect on the adsorption of nonpolar molecules such as argon or methane. However, if the nonpolar molecule has a nonzero quadrupole moment, as is the case for carbon dioxide and nitrogen, the high-pressure adsorption varies significantly as the amount of structural defects increases. In the case of polar methanol and ethanol molecules, increased hydrophilicity significantly affects adsorption, with a shift of the isotherm onset towards lower pressure values and an increase in adsorption capacity.

Table 1. Textural properties of the studied UiO-66 materials obtained from N2 and Ar adsorption as well as QE-TPDA measurements for n-hexane.

	UiO-66_220 C (ideal)	UiO-66_160 C (intermediate)	UiO-66_100 C (defected)
V_{micro} (nC6)[a]	0.239	0.271	0.329
V_{micro} (N_2)[a]	0.264	0.304	0.361
S_{BET} (N_2)[b]	1141	1271	1447
S_{BET} (Ar)[b]	1099	1198	1297

[a] micropore volume in $cm^3 \cdot g^{-1}$. [b] BET specific surface area in $m^2 \cdot g^{-1}$.

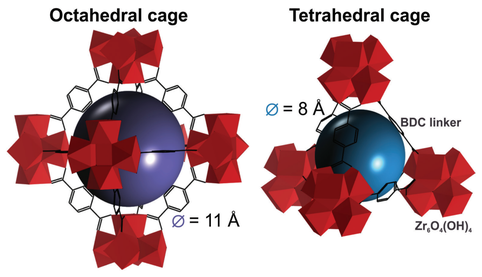

Figure 1. UiO-66 structure with octahedral (left) and tetrahedral (right) cavities marked as colored spheres. Zr polyhedrals are marked in dark red and 1,4-BDC linkers in black.

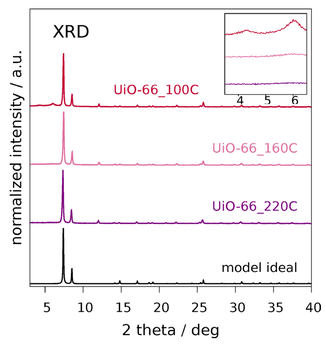

Figure 2. Powder XRD pattern of the studied UiO-66 materials.

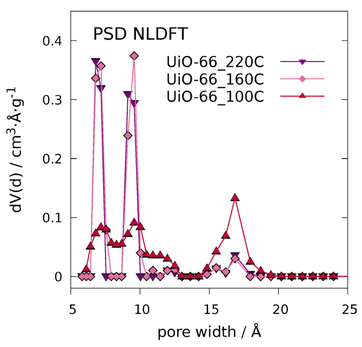

Figure 4. Pore size distribution of the studied UiO-66 preparations determined from Ar adsorption isotherms (NLDFT) measured at 87 K.

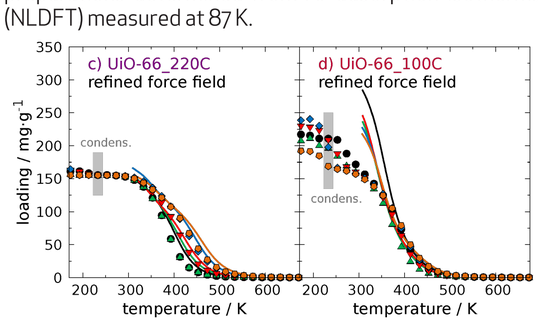

Figure 6. Experimental (lines) and GCMC (points) adsorption isobars of hexane isomers in UiO-66 for ideal (left) and defected (right) structures.

Figure 3. SEM images of the UiO-66 preparations under this study.

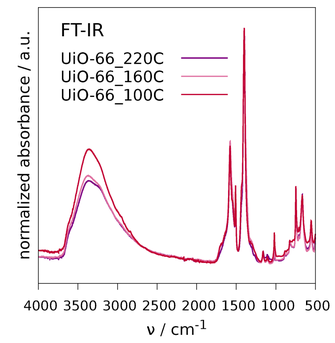

Figure 5. FT-IR absorption spectra measured for the studied UiO-66 under this study.

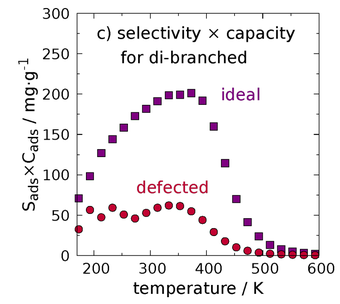

Figure 7. Temperature dependence of the product of adsorption selectivity S_{ads} and capacity C_{ads} with respect to di-branched hexane isomers (23DMB and 22DMB).

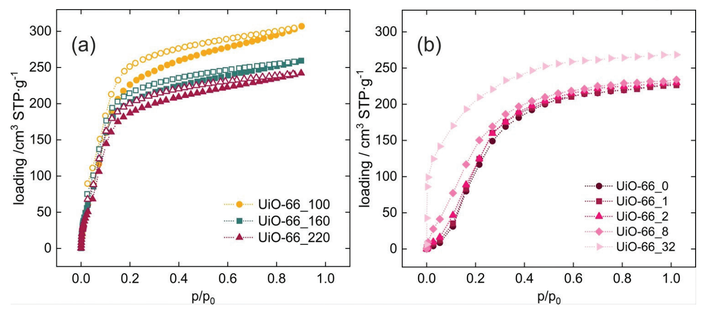

Figure 8. Experimental (a) and calculated (b) adsorption isotherms of methanol in UiO-66 measured/computed at 27 °C.

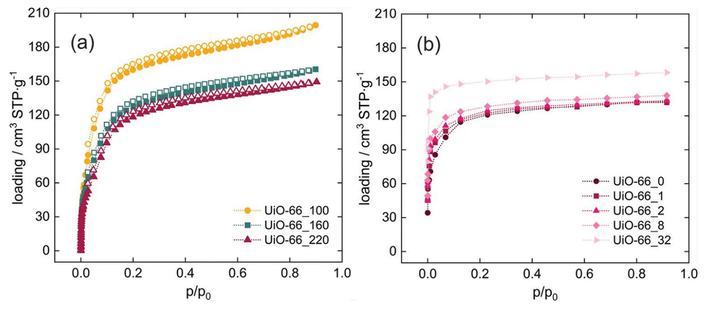

Figure 9. Experimental (a) and calculated (b) adsorption isotherms of ethanol in UiO-66 measured/computed at 27 °C.